Journal of Alloys and Compounds 1002 (2024) 175319

Contents lists available at ScienceDirect

Journal of Alloys and Compounds

journal homepage: www.elsevier.com/locate/jalcom

Luminescence under UV(A, B and C) and sunlight exposure of tetrakis Tb^{3+} carboxylate complexes doped in different polymers

Israel P. Assunção [a,b,*], Lucca Blois [a], Flora P. Cauli [a], Maria Claudia F.C. Felinto [c], Oscar L. Malta [d], Hermi F. Brito [a,**]

[a] Department of Fundamental Chemistry, Institute of Chemistry, University of São Paulo, São Paulo, SP 05508-000, Brazil
[b] Education, Science and Technology Federal Institute of São Paulo, São Paulo 01109-010, Brazil
[c] Nuclear and Energy Research Institute – IPEN/CNEN, São Paulo, SP 05508-000, Brazil
[d] Department of Fundamental Chemistry, Federal University of Pernambuco, Recife, PE 50670-901, Brazil

ARTICLE INFO

Keywords:
Lanthanide
Sunlight-emitting materials Photoluminescence
PMMA
Flufenamates
Energy transfer
LMCT

ABSTRACT

New tetrakis Lanthanide(III) carboxylate-based complexes (Ln^{3+}: Eu and Tb) were successfully synthesized via a facile one-pot method with flufenamic acid (fluf) as ligand and benzimidazole (Bzim) or 1-ethyl-3-methylimidazole (C_2mim) as counterions. In addition, the $Q[Tb(fluf)_4]$ complexes (Q^+: Bzim and C_2mim) were doped into polymethylmethacrylate (PMMA), polystyrene (PS), polycaprolactone (PCL) and poly(9-vinylcarbazole) (PVK) polymeric matrices at a 1 % (w/w) concentration and revealed highly desirable photophysical features such as wide range excitation wavelengths for the PMMA and PCL matrices and a very uncommon emission under sunlight exposure arising from the Tb^{3+} ion for the PMMA material. Thus, the tetrakis compounds with general formula $Q[Ln(fluf)_4]$ were characterized by elemental and thermal analysis, ESI-MS mass spectrometry, and FTIR absorption spectroscopy. The PMMA:(1 %)$Q[Tb(fluf)_4]$ doped films revealed higher thermal stability than the complexes. The tetrakis Eu^{3+} complex with Bzim as counterion shows no luminescence either for room or low temperature due to a highly operative low-lying ligand to metal charge transfer (LMCT) state quenching, while the corresponding C_2mim-based analogous complex reveals some weak intensity emission, showing very low intrinsic quantum yield (Q_{Eu}^{Eu}) values. On the other hand, the corresponding Tb^{3+} compounds presented bright green emission for the solid-state complexes and, particularly, for the PMMA:(1 %)$Q[Tb(fluf)_4]$ doped films when excited at UVA, UVB, and UVC radiation. Moreover, when the doped PMMA films are exposed to sunlight radiation in an open external environment, a bright green emission arising from the $^5D_4 \rightarrow {}^7F_5$ transition from the Tb^{3+} ion can be seen. In this way, these optical results suggest that the PMMA:(1 %)$Q[Tb(fluf)_4]$ luminescent photonic materials can act as versatile and efficient light-converting molecular devices (LCMDs).

1. Introduction

The luminescent properties of the trivalent lanthanide ions (Ln^{3+}) are profoundly dependent on their distinguished energy level structures. Thus, the interest in such metal ions has been increasing over the last decades for several photonic applications in different areas like temperature sensors [1,2], optical markers [3,4], biomedicine [5,6], hybrid materials [7,8], as well as luminescent solar concentrators (LSCs) [9–12]. In addition, spectroscopic features such as large relative Stokes shift, relatively long emission decay times, and line-like emission profiles, enable Ln^{3+} ions to be also used as bioprobes, avoiding autofluorescence or scattering for instance in biological systems for time-resolved spectroscopy [13,14]. In this way, Near-UV (NUV) and visible excitable materials are both highly desirable features in terms of biomedical and technological applications such as light-emitting diodes (LEDs). In fact, Eu^{3+} luminescent materials [15,16] have been more applied due to their intrinsic optical probe-like feature, while Tb^{3+} compounds are significantly less used [11,17]. Moreover, in general, the interest for light-converting metal complexes and, more specifically Ln^{3+}-based organic-inorganic hybrid compounds has been increasing over the past few years [18–23].

It is noteworthy that the intraconfigurational 4 f transitions are

* Corresponding author at: Department of Fundamental Chemistry, Institute of Chemistry, University of São Paulo, São Paulo, SP 05508-000, Brazil.
** Corresponding author.
E-mail addresses: ipassuncao@ifsp.edu.br (I.P. Assunção), hefbrito@iq.usp.br (H.F. Brito).

https://doi.org/10.1016/j.jallcom.2024.175319
Received 23 March 2024; Received in revised form 30 May 2024; Accepted 23 June 2024
Available online 24 June 2024

parity (Laporte) forbidden and, in this way, present rather low absorptivity coefficients. On the other hand, Weissman's study [24] in 1942, revealed that this spectroscopic disadvantage could be overcome by employing organic ligands that can absorb incoming radiation and transfer it to the Ln^{3+} ion. Thus, one of the most common organic ligand-to-Ln^{3+} metal ion (L → Ln^{3+}) intramolecular energy transfer (IET) mechanisms involves the absorption of light by the organic moiety (in the case of coordination compounds) from the ground to an excited singlet state ($S_0 \rightarrow S_n$) [25]. Subsequently, the energy is transferred by intersystem crossing (ISC) to a lower triplet state ($S_1 \rightarrow T_1$). Finally, the T_1 state non-radiatively transfers the energy to the Ln^{3+} emitting level, which usually exhibits light in the visible or near-infrared regions according to their energy level structure [26–28]. This luminescence process does not exclude possible energy transfer directly from the ligand singlet state to the Ln^{3+} ion. Nevertheless, competitive deactivation processes such as vibronic coupling with high energy oscillators like C-H, N-H, and mainly O-H, or even ligand to metal charge transfer (LMCT) states can depopulate the main Ln^{3+} emitting levels affecting strongly photoluminescent properties such as decay time and emission quantum yield [29–31].

Therefore, to prevent luminescence quenching by H_2O molecules commonly present in the tris species, tetrakis complexes $Q[Ln(L)_4]$, Q: counterion, and L: organic ligand [25], can be designed in which a fourth organic ligand replaces the coordinated water molecules. Moreover, the *tetrakis* species usually present improved properties when compared with the correspondent *tris* ones with the same ligand, such as higher thermal and chemical stabilities as well as higher luminescence intensity [32].

Polymers usually present interesting features like mechanical strength, relative ease and low cost of production, flexibility, and versatility [8,33]. Their uses comprise industries [34], technology [34,35], medicine [36,37], and agriculture [38,39]. Among them, polymethylmethacrylate (PMMA) is one of the most widespread kinds of synthetic polymer matrix that is employed mainly due to its excellent mechanical and spectroscopic properties [8], high light transmittance, chemical resistance, and low optical absorption in the visible range [7]. Additionally, other kinds of polymers including polystyrene (PS), polycaprolactone (PCL) and poly(9-vinylcarbazole) (PVK) can also find specific applications in different areas such as building materials, electronics, protective packing [40], 3D-printing, biomedicine (bone remodeling) [41], smart windows [42], OLEDs [43], energy storage devices and sensors [44]. Furthermore, hybrid materials formed by the doping of luminescent Ln^{3+}-complexes into polymeric matrices can generate or improve photonic properties due to their synergic effects arising from chemical interactions [8,43,45].

The organic ligand N-(3-[trifluoromethyl]phenyl)anthranilic acid, also known as flufenamic acid (Hfluf), is a derivative of the fenamic acid and belongs to the so-called non-steroidal anti-inflammatory drugs (NSAIDs). This class of pharmaceuticals is readily available for reasonable costs with analgesic, anti-inflammatory, antipyretic, and even anticancer activity [46–50]. Recently, a series of fenamic acid derivatives coordinated to Ln^{3+} ions received particular attention and among them, flufenamate (Fig. 1a) was demonstrated to be the most luminescence efficient when coordinated to the Tb^{3+} ion [11,51,52].

Herein, we report the synthesis, characterization, and photoluminescence study of tetrakis Ln^{3+} flufenamate (Eu^{3+} and Tb^{3+}) coordination compounds with C_2mim (Fig. 1b, left) and Bzim (Fig. 1b, right) as counterions. Furthermore, the tetrakis Tb^{3+}-flufenamate complexes were doped into polymeric matrices (PMMA, PS, PCL, and PVK) in a 1 % weight concentration. The terbium complexes and the doped polymeric materials showed a remarkable excitation range in the NUV-Vis region (along UVA, UVB, and UVC) or under sunlight exposure (for the PMMA films), which is a rather uncommon phenomenon for Tb^{3+}-containing materials, as recently pointed by our research group [11].

Also, it is noteworthy that Ln^{3+}-tetrakis species based on carboxylate ions are very scarce in the literature [53–55], possibly due to the inherent tendency of this organic group to form coordination polymers [56–60]. Besides the synthesis of uncommon Ln^{3+} tetrakis carboxylate systems, we aim to achieve a deeper understanding of the sunlight exposure optical phenomenon when the Tb^{3+}-based tetrakis complexes are embedded in different polymeric matrices for potential applications.

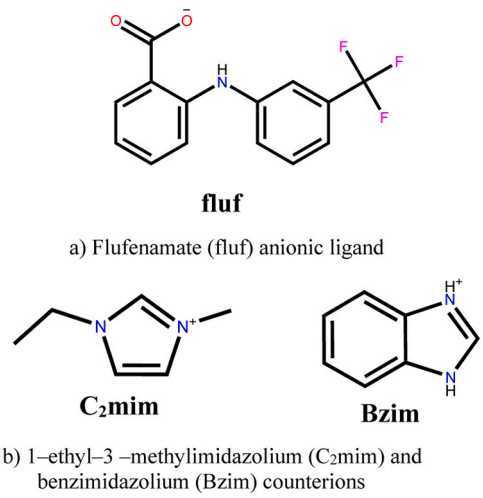

a) Flufenamate (fluf) anionic ligand

b) 1–ethyl–3 –methylimidazolium (C_2mim) and benzimidazolium (Bzim) counterions

Fig. 1. Molecular structures of a) flufenamate anion ligand and b) C_2mim and Bzim counterions.

2. Materials and methods

2.1. Preparation of the $Q[Ln(fluf)_4]$ complexes and doped polymeric films

2.1.1. Synthesis of the $Q[Ln(fluf)_4]$ complexes

Hfluf ligand, Bzim, and C_2mimBr reactants were used without further purification. $Eu(NO_3)_3$•5 H_2O were synthesized according to the literature [61] by dissolving the Eu_2O_3 in concentrated HNO_3 with heat until pH ~ 6. The mixture was filtered, and the solvent evaporated leading to a crystalline solid that was dried and stored in a desiccator under reduced pressure. On the other hand, although the Tb $(NO_3)_3$•5 H_2O was synthesized similarly, it is noteworthy that, once Tb_4O_7 is a mixed oxide, hydrogen peroxide H_2O_2 must be added to the mixture for the reduction of the Tb^{4+} to Tb^{3+} species, until obtaining a homogeneous system.

The fluf ligand was previously neutralized in isopropanol (i-PrOH) with a concentrated NH_4OH aqueous solution and reacted with the Ln^{3+} ion and counterion (Bzim or C_2mimBr) in a 5:1:1 ratio. The Ln^{3+} *tetrakis* flufenamate complexes were obtained by the dropwise addition of a Ln $(NO_3)_3$•5 H_2O aqueous solution to a mixture of the previous deprotonated ligand and the corresponding counterion source. The resulting solution was stirred at 80 °C, yielding a solid after the almost complete evaporation of the solvent. The final product was then filtered off, washed with cold i-PrOH and distilled H_2O, and stored under reduced pressure. The Ln^{3+} tetrakis flufenamate complexes with general formula $Q[Ln(fluf)_4]$, where Q stands for C_2mim and Bzim counterions are insoluble in water, but soluble in organic solvents such as methanol, ethanol, isopropanol (hot), acetone, dimethylsulfoxide (DMSO), petroleum ether, and chloroform.

2.1.2. Synthesis of the doped films polymer:(1 %)$Q[Tb(fluf)_4]$

The PMMA, PS, PCL, and PVK polymeric films doped with the Tb^{3+} tetrakis flufenamate complexes were obtained using $CHCl_3$ as solvent. Firstly, 500 mg of the corresponding polymer was dissolved in 50 mL of $CHCl_3$ at 60 °C. After, 5 mg of $Q[Tb(fluf)_4]$ was added to the mixture to obtain a 1 % solution (w/w). Subsequently, the homogeneous mixture was heated and stirred for 1 hour and poured into a Petri dish and the

excess of solvent was removed at 60 ºC, yielding the doped polymeric system. The doped films containing the tetrakis Tb^{3+} complexes presented bright green color emission under irradiation in the UVA, UVB, and UVC ranges at 405, 310, and 254 nm, respectively as well as when exposed to sunlight irradiation, for the PMMA films.

2.1.3. Methods

The elemental analyses of the lanthanide complexes were performed in Perkin-Elmer CHN 2400 instruments. The ESI-MS spectra were recorded in a Bruker Daltonics Microtof Mass Spectrometer with ESI source and TOF detection, using a 4500 V electrospray ionization source underflow of hot N_2 gas (180°C, 4 L min^{-1}) and the solid sample was dissolved in MeOH. FTIR spectra were measured in ATR mode with a Perkin-Elmer Frontier spectrometer from 4000 to 600 cm^{-1} with a spectral resolution of 4.0 cm^{-1} using a $LiTaO_3$ detector and a total of 20 scans. The thermogravimetric analysis (TG) was performed from 30 to 900 °C on a 2950 TGA HR V5.4 A under a dynamic synthetic air atmosphere of 50 $cm^3 \cdot min^{-1}$ with a constant heating rate of 10°Cmin^{-1}.

The excitation and emission spectra of the Eu^{3+} and Tb^{3+} complexes in solid state at room temperature (~ 300 K) were recorded at an angle of 22.5° (front face) with a spectrofluorometer (Horiba Fluorolog 3) with a single grating between 0.5 and 2.0 mm monochromator (SPEX1680), and the excitation source was a 450 W Xenon lamp. All spectra were recorded using a detector mode correction. The emission spectra of the Q[Tb(fluf)$_4$] complexes and the corresponding PMMA doped films under sunlight irradiation were recorded using an Optical Fiber (diameter 1 mm) connected to an Ocean Optics QE65000 spectrometer with resolution up to 1 nm. The luminescence decay curves of the emitting levels of the Q[Tb(fluf)$_4$] species were obtained at room temperature, using a phosphorimeter SPEX 1934D accessory coupled to the spectrofluorometer.

3. Results and discussion

The elemental analysis of the C, H, and N content of the Q[Ln(fluf)$_4$] complexes, where Q: C_2mim and Bzim, while Ln^{3+}: La, Eu and Tb, revealed a metal-to-ligand ratio of 1:4, suggesting the formation of the lanthanide tetrakis species (Table S1).

The ESI(+) MS data (Figure S1, S3) for the Q[Eu(fluf)$_4$] complexes revealed peaks at m/z = 119.0611 (theor. m/z = 119.0609) and m/z = 111.0924 (theor. m/z = 111.0924) arising from the $Bzim^+$ and C_2mim^+ cations, respectively, while the corresponding values for the Tb^{3+} complexes (Figure S5, S7) were m/z = 119.0607 (theor. m/z = 119.0607) and m/z = 111.0921 (theor. m/z = 111.0924) for the same counterions, respectively. The ESI(−) MS showed peaks/signals/ions at m/z = 1273.1629 and m/z = 1273.1643 (theor. m/z = 1273.1554) for the $[^{151}Eu(fluf)_4]^-$ anionic species in the $Bzim^+$ and C_2mim^+ complexes (Figure S2, S4), respectively. For the Tb^{3+} analogous complexes, were found the values m/z = 1279.1535 and m/z = 1279.1632 (theor. m/z = 1279.1595) for the $[Tb(fluf)_4]^-$ anionic complex, respectively for complexes containing $Bzim^+$ and C_2mim^+ as counterions (Figure S6, S8). These spectrometric results suggest thus, the formation of the Q[Ln(fluf)$_4$] tetrakis species either for the Eu^{3+} or Tb^{3+} ions. The isotopic patterns suggest the formation of a 2•$[Eu(fluf)_4]^-$ adduct during the ionization process (Figure S2, S4). The negative mode spectra for the Tb^{3+} complexes also show the formation of adducts but to a lesser extent.

The thermogravimetric (TG) curves (Fig. 2) of the tetrakis Tb^{3+}-flufenamate complexes were recorded in the temperature interval from 30 to 900 ºC. It is noteworthy that PMMA:(1 %)Q[Tb(fluf)$_4$] materials revealed the most promising optical properties among the polymers under consideration in this study, as will be discussed in the proper section. Thus, the thermal study of the polymers will be centered in the doped PMMA ones, and the measurements were carried out under the same experimental conditions as those of the Tb^{3+} complexes.

It is noteworthy that a precise assignment of the released species along the thermal events, is an effortful task without a TG-MS equipment and is beyond the scope of this study. Thus, the aim of the thermogravimetric investigation is to obtain information about the thermal stability of the complexes as well as the doped polymeric films.

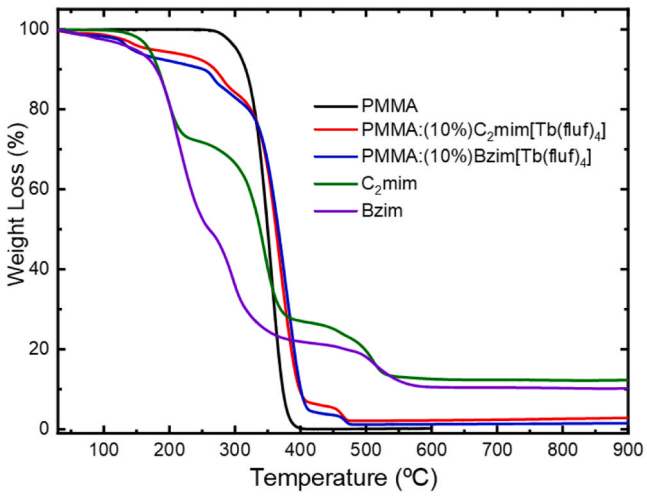

Fig. 2. TG curves of the Q[Tb(fluf)$_4$] complexes, their corresponding PMMA doped films at 1 % (w/w), and the undoped PMMA polymer. All data were obtained under a dynamic synthetic air atmosphere, of 50 $cm^3 \cdot min^{-1}$ with a constant heating rate of 10 ºC·min^{-1} from 30 to 900 ºC.

Concerning the terbium complexes Q[Tb(fluf)$_4$], the one containing the C_2mim^+ counterion showed higher thermal stability in comparison with the $Bzim^+$ based one (Fig. 2) for the first thermal decomposition event from 30 to 120 ºC, possibly due to stronger intermolecular interactions arising from the alkyl side chains of the C_2mim^+ group that is less likely in the Bzim[Tb(fluf)$_4$] complex. In general, for both tetrakis species, the thermal decomposition path occurs in three overlapped steps. The first one takes place from 40 to 250 ºC and accounts for the loss of ~28 and ~51 %, while in the second decomposition step from 225 to 400 ºC, the mass loss corresponds to ~45 and 28 % for the C_2mim and Bzim-based counterions, respectively. Finally, the last thermal event accounts for 14 and 11 % of mass loss in the 460–625 ºC interval for both systems. Considering the remaining mass, the residue product is possibly the mixed terbium oxide, Tb_4O_7, independently of the counterion. It is noteworthy that the mass loss values and the decomposition pathway are significantly different from the previously reported TG curves for the corresponding tris species [11]. The polymeric films doped with the Tb^{3+} complexes revealed higher thermal stability when compared to the complexes in the solid state (Fig. 2).

FTIR absorption spectra of the Bzim[Tb(fluf)$_4$] complexes (Figure S9, left) revealed two middle-intensity peaks at 3490 and 3295 cm^{-1} attributed to N – H stretching mode from the bridge secondary amine group. Considering that the Hfluf free ligand showed the corresponding N – H vibrational mode at 3325 cm^{-1}, the shift of this frequency towards a higher wavenumber suggests the coordination of the N atom to the Ln^{3+} ion in contrast with other fenamate tris species [51,61–63], but in good agreement with other carboxylate-based tetrakis species containing an N or O atom close to the COO^- group [55]. It seems reasonable to assume the participation of a neighboring atom, such as the N in the flufenamate ligand, once it leads to the formation of a more stable 6-member ring upon the coordination to the metal ion, instead of a high energy 4-member ring formed in a "purely" carboxylate coordination. Also, the absorption band at 3295 cm^{-1} can be assigned to a NH group from a polymorphic form of the flufenamate anion [64,65]. Nevertheless, it is possible to observe that the N – H mode is overlapped with a broad band from 3700 to 3100 cm^{-1} for the C_2mim[Tb(fluf)$_4$] complex (Figure S9, right), suggesting the formation of hydrogen bonding interactions involving the C_2mim^+ counterion, once no similar feature is

observed for the $Bzim^+$-based compound. In addition, the strong absorption peaks from 3100 to 2800 cm^{-1} in the C_2mimBr free species were almost completely suppressed, suggesting that the C_2mim^+ species is involved in new chemical interactions. Such experimental observation corroborates with the thermogravimetric data that could confirm the higher thermal stability of the C_2mim^+-based complex. The high-intensity peak at 1660 cm^{-1} in the Hfluf ligand is no longer seen in the Q[Tb(fluf)$_4$] complexes. Conversely, in the coordination compounds, two new bands are observed at around 1610 and 1400 cm^{-1} corresponding, respectively, to the asymmetric (ν_{as}) and symmetric (ν_s) stretching modes of the carbonyl group, suggesting, thus, its effective coordination to the Ln^{3+} ion. The difference between the ν_{as} and ν_s modes, *i.e.* $\Delta\nu$, the comparison between this value for the solid-state complexes and a corresponding Na^+ or K^+ salt gives information about the carbonyl group coordination mode [66]. Hence, once the $\Delta\nu$ for the complexes is lower but very close to the corresponding value for the Nafluf salt, it is possible to infer that the flufenamate ligand is coordinated to the Ln^{3+} ion via a bridge-type or chelate-type coordination mode, as observed for the tris species [11,51,52].

4. Luminescence study

4.1. Photoluminescence investigation of europium tetrakis complexes Q[Eu(fluf)$_4$]

To investigate the origin of the distinguishing yellowish color of the Q[Eu(fluf)$_4$] (Q^+: Bzim and C_2mim) in contrast with the whitish powder for the analogous systems containing other Ln^{3+} ions such as La^{3+} or Tb^{3+}, the diffuse reflectance spectra of the Eu^{3+} complexes and the corresponding La^{3+}-based ones were recorded at room temperature from 300 to 800 nm (Fig. 3a,b).

As one can see, there is a broad and intense band in the Q[Eu(fluf)$_4$] spectra that is absent in the Q[La(fluf)$_4$] (Fig. 3a,b) and the arithmetic difference between each of the points in the Eu^{3+} complexes spectra and the corresponding La^{3+} ones corresponds to a ligand-to-metal charge transfer state (LMCT) observed in the Eu^{3+} complexes (green curve in the inset in Fig. 3a,b) and is the main responsible for the yellowish color of these materials (Fig. 3c-f), conversely to the La^{3+}-based analogues. Such optical data are in good agreement with previous results for corresponding tris Ln^{3+} flufenamates [11]. The fact that only the C_2mim[Eu(fluf)$_4$] complex presents some emission intensity, is an indication of a less operative quenching by the LMCT state, due to the higher energy of the LMCT transition. In this way, the complex containing the C_2mim^+ counterion presents a lesser luminescence quenching contribution that is corroborated by its fainter yellowish color when compared to those of the Bzim[Eu(fluf)$_4$] (Fig. 3c-f) and [Eu(fluf)$_3$(H$_2$O)] complexes [11].

Differently from the tetrakis terbium complexes Q[Tb(fluf)$_4$], the corresponding Eu^{3+} ones are practically non-luminescent at room temperature. The excitation spectra of the Q[Eu(fluf)$_4$] complexes (Q^+: Bzim and C_2mim) were recorded at 300 K (Fig. 4a) and low temperature (Fig. 4b) from 250 to 525 nm monitoring the emission at Eu^{3+} hypersensitive transition $^5D_0 \rightarrow {}^7F_2$ (~ 617 nm). The excitation spectra revealed a broad band from 350 to 425 nm assigned to the intraligand $S_0 \rightarrow S_1$ transition with moderate intensity and a narrow peak at 464 nm arising from the $^7F_0 \rightarrow {}^5D_2$ transition of the Eu^{3+} ion. It is noteworthy that the excitation spectra of the [Eu(fluf)$_3$(H$_2$O)] complex do not exhibit excitation bands (Fig. 4a-b, black line).

The excitation spectra of the tetrakis species are significantly different from each other at 300 K, but similar at low temperature, and the C_2mim[Eu(fluf)$_4$] complex showed higher relative excitation intensity than the Bzim[Eu(fluf)$_4$] (Fig. 4a,b) in the 300–425 nm range. Due to the operative LMCT energy transfer of the Q[Eu(fluf)$_4$] complexes, the excitation band intensities centered on the organic ligand in the Eu^{3+} complexes are significantly lower than those of the

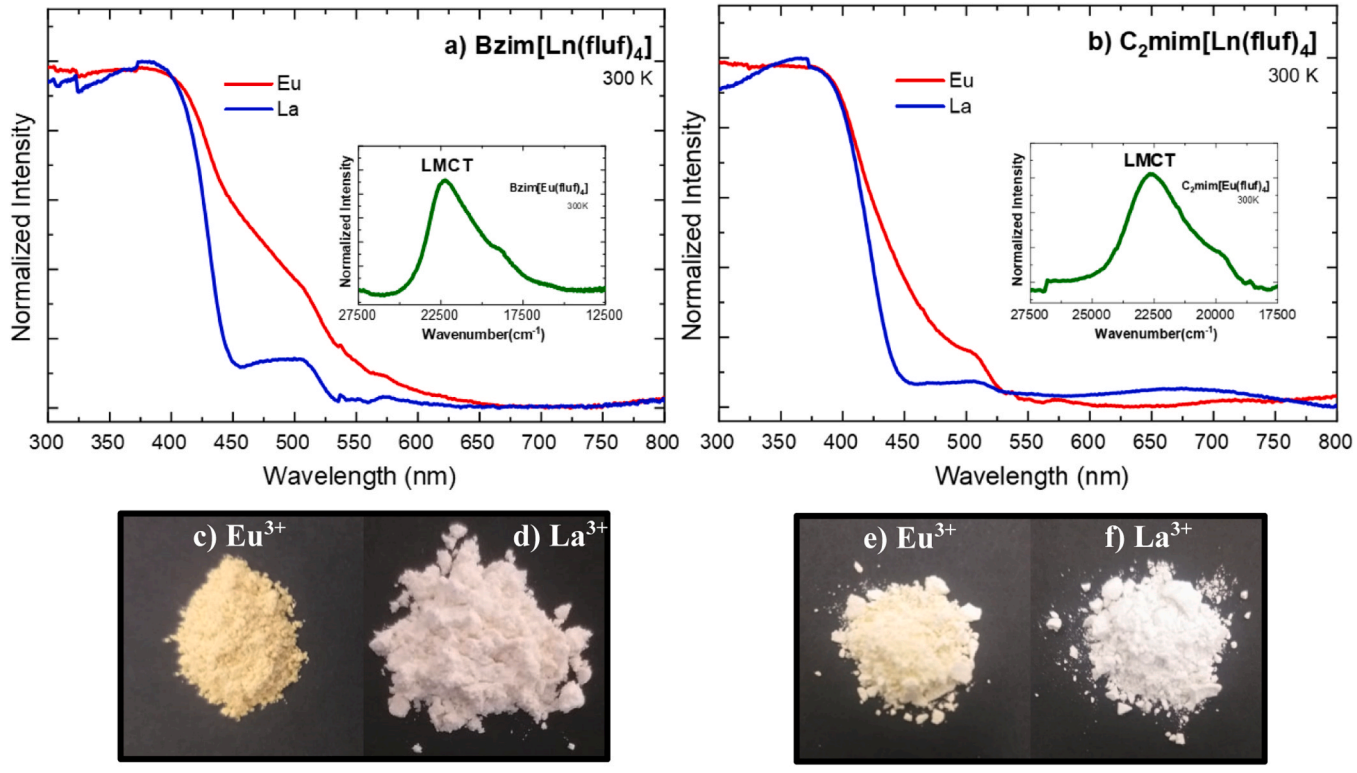

Fig. 3. Diffuse reflectance spectra of the Q[Ln(fluf)$_4$] compounds, where Q^+: Bzim (a) and C_2mim (b), while Ln: La^{3+} (blue line) and Eu^{3+} (red line) registered at room temperature (~ 300 K). The inset figure shows the LMCT band (green curves) generated by the arithmetic difference between the Eu^{3+} and La^{3+} spectra. The photographs correspond to the Eu^{3+} tetrakis complexes with $Bzim^+$ (c) and C_2mim^+ (e) countercations (yellowish powders), while the corresponding La^{3+}-based ones are depicted in (d) and (f) for the same countercations (whitish powders), respectively under ambient light.

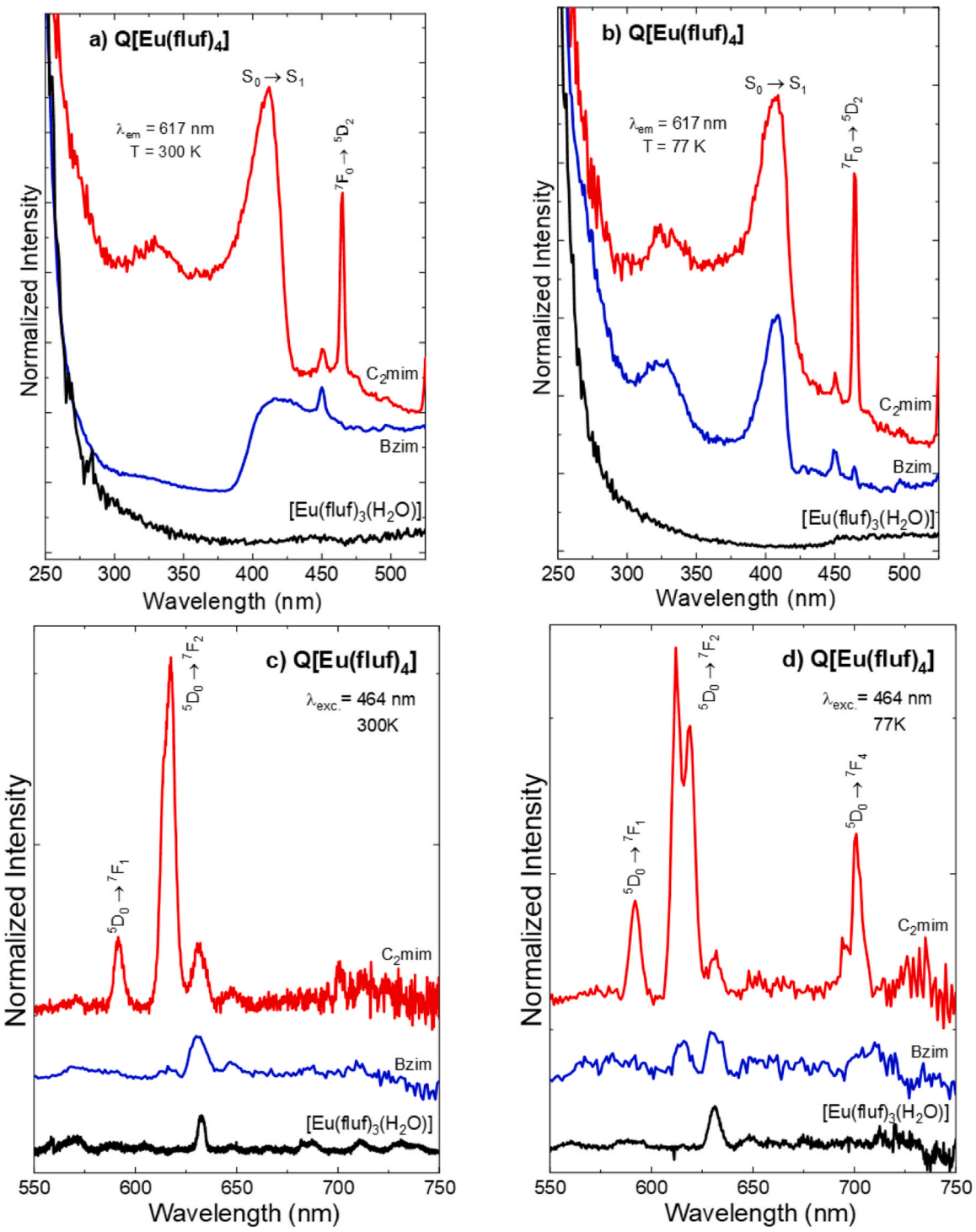

Fig. 4. Excitation spectra of the solid-state Q[Eu(fluf)$_4$] complexes, where Q = Bzim$^+$ and C$_2$mim$^+$ recorded under room temperature (a) and 77 K (b) in the 250 – 525 nm range monitoring the emission at the $^5D_0 \rightarrow {}^7F_2$ transition ($\lambda_{em.}$ = 617 nm) of the Eu^{3+} ion. Emission spectra of the solid-state Q[Eu(fluf)$_4$] complexes, where Q$^+$: Bzim and C$_2$mim recorded under room temperature (c) and 77 K (d) in the 550 – 750 nm range with excitation at 464 nm centered on the Eu^{3+} ion.

corresponding Tb^{3+} ones. Moreover, the complete absence of excitation bands in the tris [Eu(fluf)$_3$(H$_2$O)] complex (Fig. 4a,b, black line) is due to the operative LMCT states for depopulating both ligand states and Eu^{3+} levels as reported in reference [11].

The emission spectra of the Q[Eu(fluf)$_4$] compounds (Q$^+$: C$_2$mim and Bzim) and the corresponding tris species were recorded from 550 to 750 nm with excitation centered on the Eu^{3+} ion at 464 nm under room temperature and 77 K (Fig. 4c,d). In general, the low-temperature spectra of the tetrakis species with the same counterion presented a slightly higher emission intensity than the room temperature measurement, better spectral resolution and the electric dipole hypersensitive $^5D_0 \rightarrow {}^7F_2$ transition (~ 617 nm) [14] was the most intense for both temperatures. It is noteworthy that the emission spectra of the Eu^{3+} complexes were also registered with excitation at 410 nm, but the relative intensity of the emission bands were comparatively lower than those obtained when excited at 464 nm and were thus not shown.

Interestingly, the C$_2$mim[Eu(fluf)$_4$] complex showed significantly higher intensity than the corresponding Bzim$^+$-based complex,

suggesting a possible participation of the counterion in the energy transfer process. In fact, the presence of the C_2mim^+ and $Bzim^+$ counterions in the tetrakis compounds seems to play a role in the coordination geometry around the Eu^{3+} ion, contributing to the relative energy position of the LMCT state. The relative position of the LMCT band of the tetrakis Eu^{3+}-based complexes seems to be temperature-dependent, as already observed for other systems [67–69] including hydrated and tris-substituted Eu^{3+} flufenamates [11].

The experimental intensity parameters (Ω_2 and Ω_4) values for the solid-state $C_2mim[Eu(fluf)_4]$ complex (Table 1) were calculated according to Eq. 1 since this Eu^{3+} complex is the only one that presents sufficient emission intensity:

$$A_{0\to\lambda} = \frac{4\omega^3 e^2 \chi}{3\hbar c^3}\Omega_\lambda \left|\langle {}^5D_0 \left|\left| U^{(\lambda)} \right|\right| {}^7F_\lambda \rangle\right|^2 \quad (1)$$

for which ω is the angular frequency of the transition, e is the elementary charge, χ is the Lorentz local field correction factor, $\hbar$ is the reduced Planck constant and c is the speed of light. The quantities $\left|\langle {}^5D_0 \left|\left| U^{(\lambda)} \right|\right| {}^7F_\lambda \rangle\right|^2$ are the squared reduced matrix elements whose values are equal to 0.0032 and 0.0023 for $\lambda = 2$ and 4, respectively [70, 71].

The values for χ were determined using $n = 1.5$ [72] as the index of refraction. It is noteworthy that recent studies revealed a higher sensitivity of the Ω_2 parameter to even small angular variations, while the Ω_4 values are more sensitive to the distance variations between ligand atom and Eu^{3+} ion [73,74].

The experimental values for the spontaneous emission coefficients ($A_{0\to J}$) related to the ${}^5D_0 \to {}^7F_{1,2,4}$ transitions of the Eu^{3+} ion were determined using Eq. 2 [26,71,75] from the emission spectra of the $C_2mim[Eu(fluf)_4]$ compound:

$$A_{0\to J} = \left(\frac{S_{0\to J}}{S_{0\to 1}}\right) A_{0\to 1} \quad (2)$$

where $S_{0\to 1}$ and $S_{0\to J}$ stands for the areas under the emission curves of the ${}^5D_0 \to {}^7F_1$ and ${}^5D_0 \to {}^7F_{2,4}$, respectively [75]. Moreover, once the ${}^5D_0 \to {}^7F_1$ transition is almost completely governed by the magnetic dipole (MD) mechanism and its intensity is practically insensitive ($n = 1.5$, $A_{0\to 1} \sim 50\ s^{-1}$) [75] to the chemical environment around the Eu^{3+} ion, such transition is frequently used as an internal reference to obtain the $A_{0\to J}$ values.

The intrinsic emission quantum yield (Q_{Eu}^{Eu}) [72,75] is defined as the ratio between the radiative (A_{rad}) and the total (A_{total}) decay rates that are given by the sum of radiative and non-radiative (A_{nrad}) rates (Eq. 3). In addition, Eq. 4 [72] shows the relationship between A_{total} rate and the emitting ${}^5D_0$ level lifetime (τ_{obs}) in which the τ_{obs} values were calculated from their luminescence decay curves. By its turn, such curves were obtained by monitoring the emission at the ${}^5D_0 \to {}^7F_2$ transition (617 nm) under excitation at the ${}^7F_0 \to {}^5D_2$ transition (464 nm) at 300 and 77 K.

$$Q_{Eu}^{Eu} = \frac{A_{rad}}{A_{rad} + A_{nrad}} \quad (3)$$

$$\tau_{464} = \frac{1}{A_{rad} + A_{nrad}} = \frac{1}{A_{total}} \quad (4)$$

The values of the Ω_2 and Ω_4 intensity parameters of the $C_2mim[Eu(fluf)_4]$ complex were obtained at 300 and 77 K (Table 1). On the other hand, the corresponding data for the $Bzim[Eu(fluf)_4]$ complex were not calculated due to the absence of luminescence at both temperatures.

The Ω_2 parameter is relatively small and reflects the low intensity of the ${}^5D_0 \to {}^7F_2$ hypersensitive transition of the Eu^{3+} ion. In addition, the value under 77 K is slightly higher than at 300 K, suggesting a higher angular variation around the Eu^{3+} ion as the temperature decreases. The Ω_4 values, on the other hand, are practically the same, and thus, one can infer that the Eu^{3+} - L bond distances are almost unaffected by the change in temperature. It is worth mentioning that the Ω_4 values for the tetrakis complex under consideration in this investigation is very similar to the values found in the ternary tris ones reported by our group [11], indicating the major contribution of the fluf anion to ligand to metal bond distances. We should note that the measured Ω_4 value at room temperature differs from that at 77 K due to the difficulty in the detection of the ${}^5D_0 \to {}^7F_4$ transition.

Concerning the values of the A_{rad} rate under both temperatures, only a small effect is observed upon cooling down, once the values are essentially the same (Table 1). Conversely, the A_{nrad} rate is significantly affected by lowering the temperature due to a decrease in vibronic contributions with high energy oscillators like C–H, N–H, and mainly O–H [15,76] and a decrease in the luminescence quenching due to the LMCT state. Table 1 also reveals a consequent increase in the emission lifetime value as the temperature decreases, reinforcing the role of the LMCT state as an efficient suppressing channel.

Finally, a higher intrinsic quantum yield value at low temperature ($Q_{Eu}^{Eu} = 32\ \%$) when compared to that recorded at room temperature ($Q_{Eu}^{Eu} = 5.4\ \%$) is due to the lower nonradiative contribution of A_{nrad} ($1030\ s^{-1}$) at 77 K. Once again, these spectroscopic results are close to those found for the tris species [11] and point out that flufenamate ion is the main responsible for the optical features of these materials.

4.2. Photoluminescence study of terbium complexes Q[Tb(fluf)$_4$] and the doped polymeric films

The photophysical properties were investigated by the excitation spectra of the tetrakis $Q[Tb(fluf)_4]$ (Q: $Bzim^+$ and C_2mim^+) and the tris $[Tb(fluf)_3(H_2O)]$ complexes doped in PMMA, PCL, PS, and PVK polymeric films (Fig. 5a-c). These spectra were recorded at room temperature (~ 300 K) in the 250–525 nm range monitoring the emission at the ${}^5D_4 \to {}^7F_5$ transition of the Tb^{3+} ion (543 nm).

When we consider the tetrakis and tris Tb^{3+} complexes (Fig. 5a), their optical data reveal intense and broad excitation bands in the UVA, UVB, and UVC ranges centered at the organic ligand and assigned to the $S_0 \to S_n$ transitions of flufenamate anion. The excitation bands exhibit similar spectral profiles, although, when one compares the excitation band of the tetrakis species with the analogous tris one (Fig. 5a), the former showed a slight broadening to longer wavelengths.

The excitation spectra of the polymeric films doped with the Q[Tb(fluf)$_4$] (Fig. 5b,c) and $[Tb(fluf)_3(H_2O)]$ (Figure S10) also present intense broad bands centered on the organic ligand and similar spectral profiles either for the tris or the tetrakis compounds. Moreover, the PS- and PVK-based materials show notably even broader excitation range, up to 440 nm when doped with $C_2mim[Tb(fluf)_4]$ complex (Fig. 5c) and 450 nm for the doped films containing the tris $[Tb(fluf)_3(H_2O)]$ species (Figure S10). Nevertheless, in the PMMA-based film doped with the tris species, the coordinated H_2O molecule is possibly released and replaced

Table 1
Experimental intensity parameters ($\Omega_{2,4}$), radiative (A_{rad}) and non-radiative (A_{nrad}) decay rates, emission lifetime (τ_{464}), and intrinsic quantum yield (Q_{Eu}^{Eu}) of the solid-state $C_2mim[Eu(fluf)_4]$ complex determined at 300 and 77 K.

Eu^{3+}-Complex/ T(K)	Ω_2 (10^{-20} cm^2)	Ω_4 (10^{-20} cm^2)	A_{rad} (s^{-1})	A_{nrad} (s^{-1})	A_{total} (s^{-1})	τ (ms)	Q_{Eu}^{Eu} (%)
$C_2mim[Eu(fluf)_4]$ (300 K)	12.8	2.8	335	5876	6211	0.161	5.4
(77 K)	10.4	7.1	332	697	1030	0.971	32

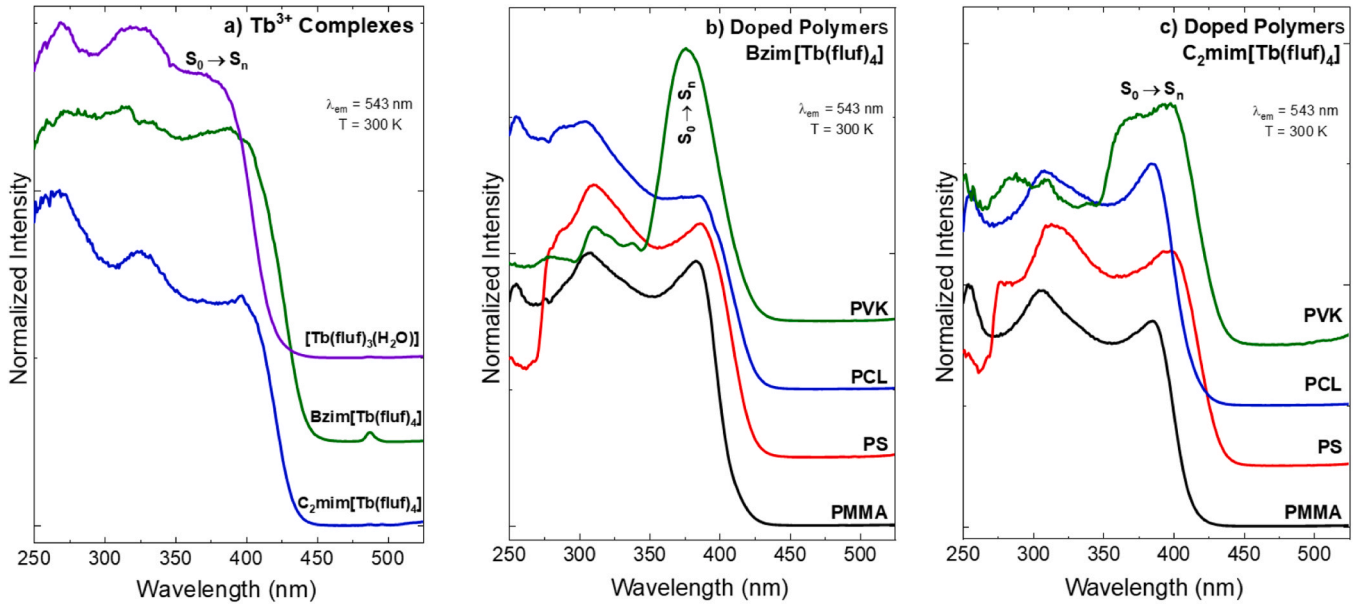

Fig. 5. Excitation spectra of the solid-state Q[Tb(fluf)$_4$] and [Tb(fluf)$_3$(H$_2$O)] complexes (a) and the corresponding polymeric films doped at 1 % (w/w) with the Q[Tb(fluf)$_4$], where Q = Bzim$^+$ (b) and C$_2$mim$^+$ (c). All spectra were recorded at room temperature in the 250 – 525 nm range monitoring the emission at the $^5D_4 \rightarrow {}^7F_5$ transition ($\lambda_{em.}$ = 543 nm) of the Tb^{3+} ion.

by the polymeric matrix via carbonyl groups as previously observed for other doped PMMA materials [33].

Emission spectra of the tris [Tb(fluf)$_3$(H$_2$O)] and tetrakis Q[Tb(fluf)$_4$] complexes (Fig. 6a) and the respective PMMA, PCL, PS, and PVK doped films with Bzim[Tb(fluf)$_4$] and C$_2$mim[Tb(fluf)$_4$] (Fig. 6b, c, respectively) were registered in the 475–700 nm range with excitation at the ligand band (390 nm) at 300 K. Concerning either the tris or the tetrakis complexes, all emission spectra revealed no broad bands arising from the organic moiety, suggesting an efficient L → Tb^{3+} energy transfer. Therefore, only narrow emission peaks are observed and were assigned to the $^5D_4 \rightarrow {}^7F_{6-3}$ intraconfigurational transitions centered on the Tb^{3+} ion, *i.e.*, $^5D_4 \rightarrow {}^7F_6$ (489 nm), $^7F_5$ (543 nm), $^7F_4$ (585 nm) and $^7F_3$ (621 nm). The $^5D_4 \rightarrow {}^7F_5$ transition is invariably the most intense and the main responsible for the bright green emission arising from the complex and the doped films. Moreover, such transition, that possess a electric and magnetic dipole nature, showed different spectral profiles for each Tb^{3+}-based species (notably for the C$_2$mim-containing one), suggesting different chemical environments around the metal ion.

In addition, their spectral profiles (Fig. 6a), and the relative emission intensities for each complex are different, suggesting unique chemical environments around the Tb^{3+} ion. Qualitatively, it is possible to observe that for the Q[Tb(fluf)$_4$] compounds, there is an influence of the counterion upon the coordination geometry. These observations reinforce the formation of the tetrakis complexes, conversely to the tris one.

The emission spectra of the PMMA, PCL, PS, and PVK films doped with the tris [Tb(fluf)$_3$(H$_2$O)] (Figure S11) and tetrakis Q[Tb(fluf)$_4$], where Q: Bzim$^+$ (Fig. 6b) and C$_2$mim$^+$ (Fig. 6c), showed that emission bands for the doped materials are broader than the corresponding

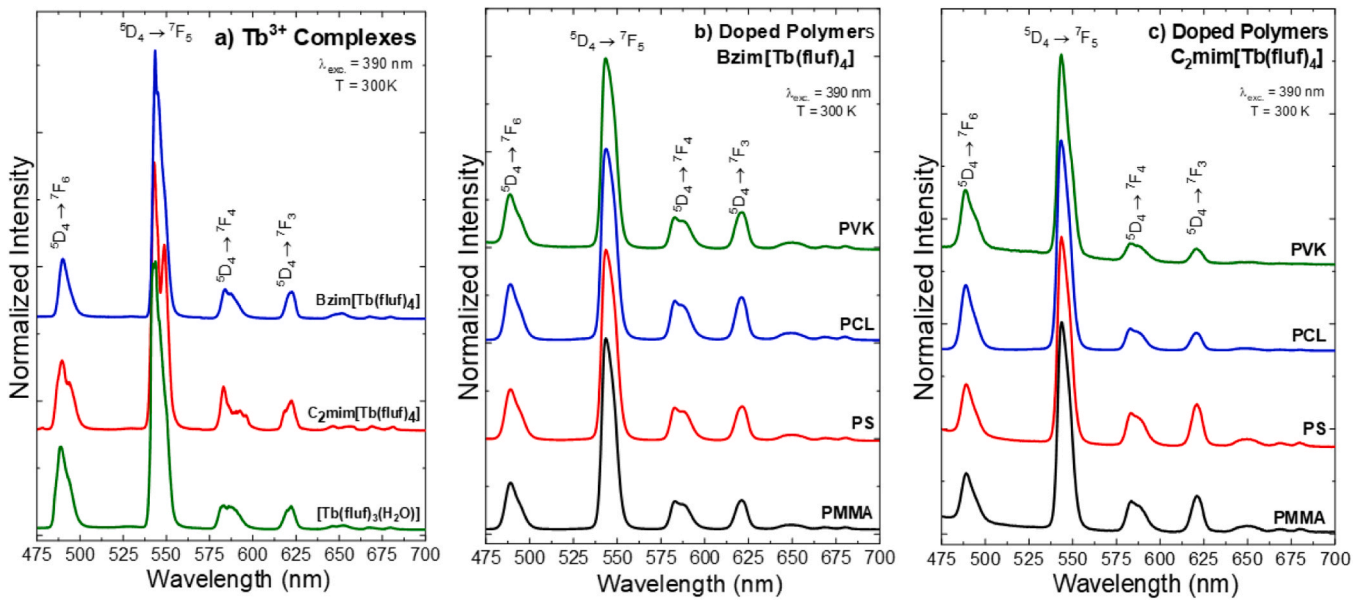

Fig. 6. Emission spectra of the tris [Tb(fluf)$_3$(H$_2$O)] and tetrakis Q[Tb(fluf)$_4$] complexes (a), as well as the corresponding polymer films doped at 1 % (w/w) with the Q[Tb(fluf)$_4$], where Q: Bzim$^+$ (b) and C$_2$mim$^+$ (c). All spectra were recorded at 300 K in the 475 – 700 nm range with excitation at 390 nm.

complexes. In general, no broad emission bands arising from the organic moiety can be seen for any of the polymers doped with tetrakis species, while the PVK- and mainly PS-based systems doped with the tris Tb^{3+} complex revealed some contribution arising from the polymer matrix (Figure S11).

Comparatively, among the doped polymers, those containing the Bzim[Tb(fluf)$_4$] complex (Fig. 6b), revealed the better energy transfer process and the most intense emission bands, while the matrices doped with the C_2mim[Tb(fluf)$_4$] and [Tb(fluf)$_3$(H_2O)] species (Fig. 6c and S11) revealed to be comparatively less efficient.

The doped polymers were also excited by sunlight irradiation and their emission spectra were recorded at room temperature (Fig. 7a-c). In the case of the emission spectra of the doped PCL, PS, and PVK films, either the tris or tetrakis complexes, all of them revealed essentially exclusively the background broad emission bands arising from the sunlight, and no narrow peaks from the Tb^{3+} ion were observed. On the other hand, the doped PMMA polymer films exhibit narrow emission peaks originating from the $^5D_4 \rightarrow {}^7F_{6-3}$ transitions of the Tb^{3+} ion (Fig. 7a-c). In addition, these photoluminescent data suggest that the tetrakis-based PMMA:(1 %)Bzim[Tb(fluf)$_4$] material is the best candidate for excitation at UVA, UVB and UVC regions, as well as for excitation under sunlight exposure, due to the absence of the solar background radiation from the emission spectrum (Fig. 7c).

In addition, the emission decay lifetimes of the doped polymers with the tetrakis Tb^{3+}-complexes increase in the following order PVK < PS < PCL < PMMA (Table S2). The highest values were invariably shown by the materials doped with the Bzim[Tb(fluf)$_4$] complex, while the lowest ones were found for the tris [Tb(fluf)$_3$(H_2O)]-doped species. Based on these observations, one can infer that, irrespective of the polymeric matrix, the Bzim[Tb(fluf)$_4$] species possibly present the most strong interactions with the host material, leading to the higher lifetime values found in this investigation. Also, the lack of a fourth fluf ligand around the Tb^{3+} ion could explain the fact of the tris species presents the lower lifetimes, no matter the host matrix constitution.

The CIE (*Commission Internationale l'Eclairage*) chromaticity coordinates were determined based on the experimental emission spectra of the Q[Tb(fluf)$_4$] complexes and their corresponding doped films, with excitation under 405 nm (UVA), 310 nm (UVB) and 254 nm (UVC), besides the exposure to the sunlight irradiation. Nevertheless, for the sake of clarity, Fig. 8 shows the results only for the doped PMMA and PCL films, while the diagram of PS and PVK polymers can be seen in Figure S12.

The inset photographs in Fig. 8 and Figure S12 were taken with a digital camera and show the green emission of the doped polymeric materials under excitation at different wavelengths and when irradiated by the sunlight in an open external environment (in the case of the PMMA matrix). As can be seen, the luminescence is rather high for the PMMA and PCL polymers (Fig. 8), while is significantly less intense for the PS and PVK-based materials (Figure S12), when these materials are excited at 405 nm (UVA), 310 nm (UVB) and 254 nm (UVC). In general, the x,y coordinates (Table S3) can be seen in the green region with some slight deviations to the yellowish including the points assigned to the sunlight irradiation spectra due to the background solar contribution in a similar manner of previously observed for other Tb^{3+} flufenamate complexes [11].

5. Conclusions

The Q[Ln(fluf)$_4$] complexes (Q^+: Bzim and C_2mim) (Ln^{3+}: Eu and Tb) and the corresponding Tb^{3+} doped films at 1 % (w/w) with PMMA, PCL, PS, and PVK polymer films were successfully prepared and characterized. The thermal stability of the complexes was improved upon doping in the PMMA polymeric matrix. The C_2mim[Eu(fluf)$_4$] complex revealed a weak luminescence either at room temperature or 77 K, which can be attributed to the presence of an operative LMCT state that quenches the emission from the Eu^{3+} ion. In addition, the higher emission intrinsic quantum yield ($\mathbf{Q}_{\mathbf{Eu}}^{\mathbf{Eu}}$) showed a significant increase of about five times as the temperature decreased. On the other hand, for the Bzim[Eu(fluf)$_4$] compound luminescence intensity is completely suppressed by the LMCT state. It is noteworthy that, the Bzim[Eu(fluf)$_4$] complex showed a higher intensity yellow color to the naked eye, under ambient light when compared to the C_2mim^+ analogous, which arises from the lower LMCT energy relative position of the former that present consequently, absolutely no emission under 300 or 77 K.

The photophysical data showed that all the doped films with the Q[Tb(fluf)$_4$] complexes can be excited over a large range of wavelengths comprising the UVA (405 nm), UVB (310 nm), and UVC (254 nm) regions, exhibiting particularly strong emission for the PMMA and PCL-based doped polymers arising from the $^5D_4 \rightarrow {}^7F_{6-3}$ transitions of the Tb^{3+} ion. Besides, the PMMA:(1 %)Q[Tb(fluf)$_4$] materials showed a

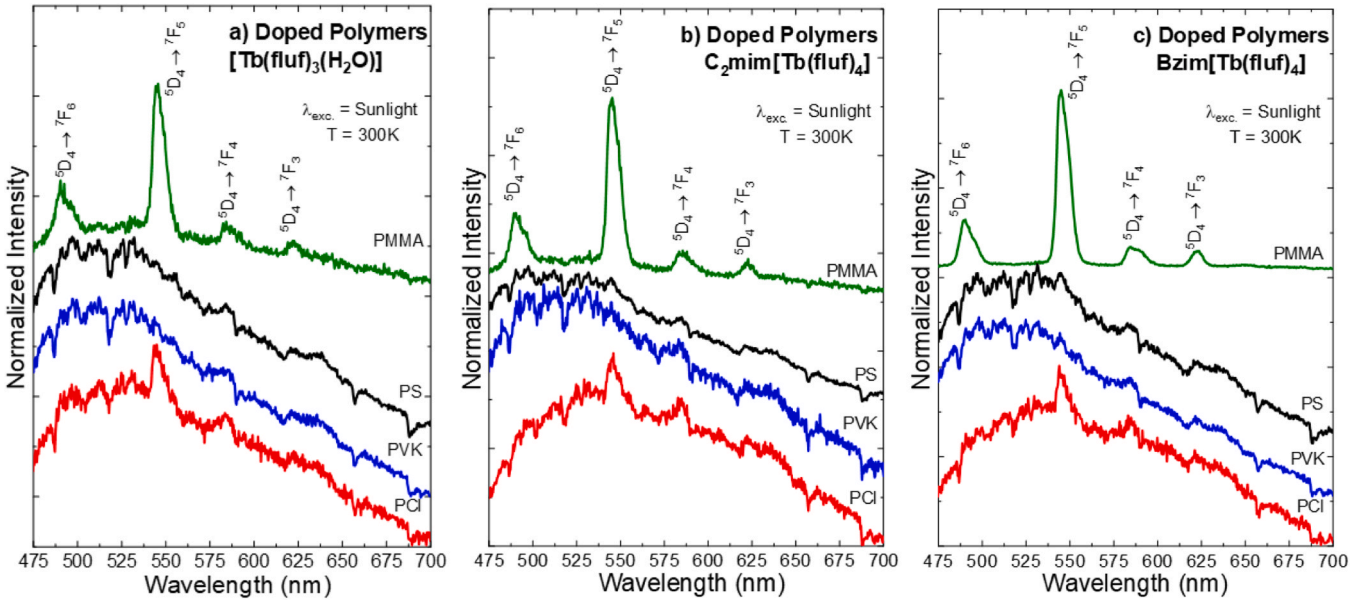

Fig. 7. Emission spectra of the doped films with the tris [Tb(fluf)$_3$(H_2O)] (a) and tetrakis Q[Tb(fluf)$_4$] complexes, where Q: C_2mim^+ (b) and $Bzim^+$ (c). All spectra were recorded at 300 K in the 450 – 700 nm range under excitation by the sunlight exposing the films in an open external environment.

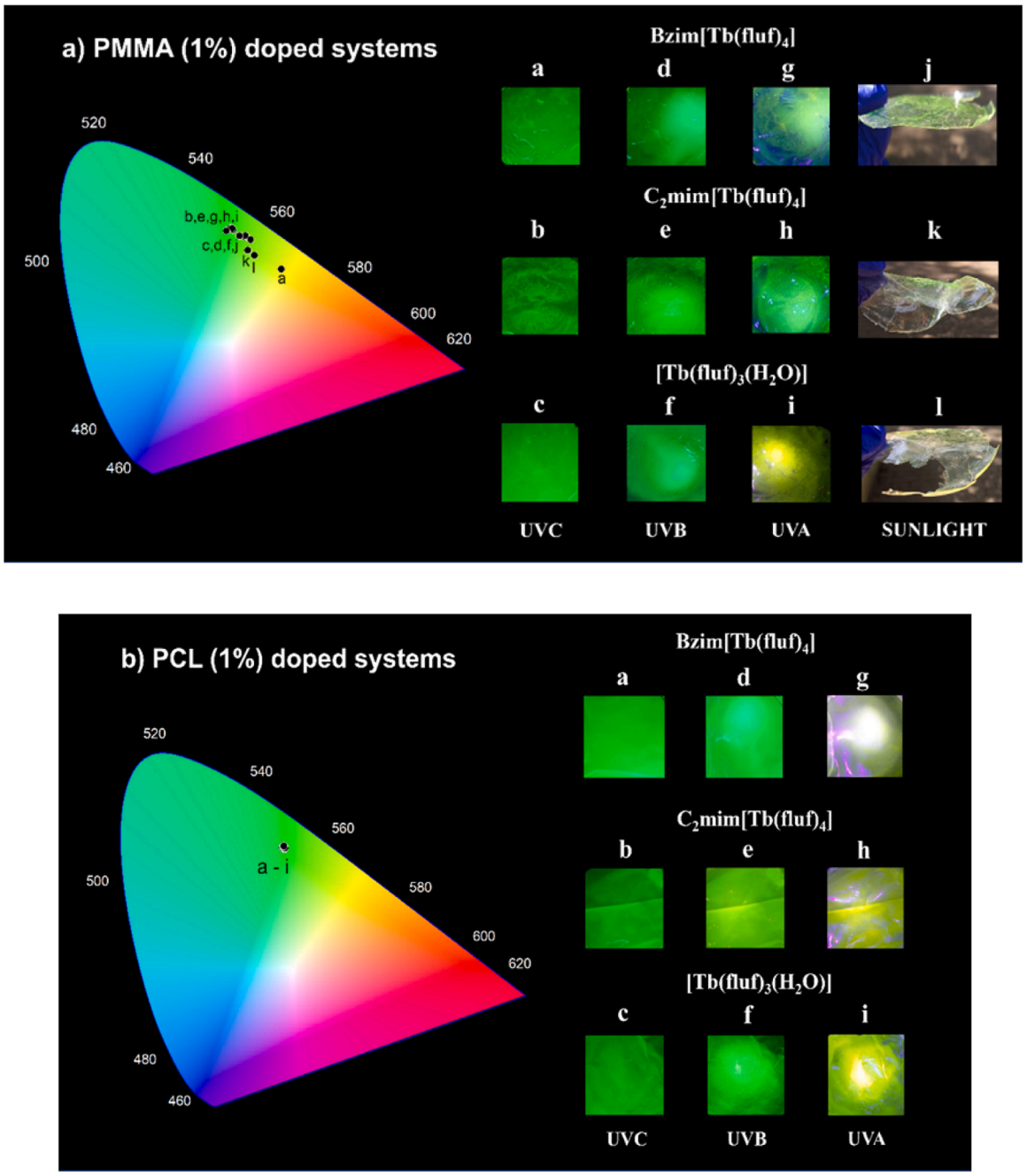

Fig. 8. CIE diagram for the PMMA (top) and PCL (bottom) doped films containing the tris $[Tb(fluf)_3(H_2O)]$ and tetrakis $Q[Tb(fluf)_4]$ complexes at 1 % (w/w) obtained from their emission spectra at 254 (a-c), 310 (d-f) and 405 nm (g-i), as well as under sunlight exposure (j-l). All spectra were registered at room temperature. The inset figures show digital photographs of the films and their green emission color under different excitation sources.

remarkable green emission when the films were exposed to sunlight radiation in an open external environment. In this way, the doped polymers were revealed to be versatile photonic materials with a wide excitability range, including near UV and beyond, and with possible different applications such as bioprobes, and light-converting molecular devices (LCMDs).

CRediT authorship contribution statement

Israel P. Assunção: Conceptualization, Spectroscopic Investigation, Formal analysis, Investigation, Methodology, Writing – original draft, Writing – review & editing. **Lucca Blois:** Conceptualization, Spectroscopic Investigation, Formal analysis, Investigation, Methodology, Writing – original draft, Writing – review & editing. **Flora P. Cauli:** Methodology, Writing – review & editing. **Maria Cláudia F. C. Felinto:** Conceptualization, Spectroscopic Investigation, Formal analysis, Funding acquisition, Project administration, Resources, Supervision, Writing – review & editing. **Oscar L. Malta:** Conceptualization, Spectroscopic Investigation, Formal analysis, Supervision, Writing – review & editing. **Hermi F. Brito:** Conceptualization, Spectroscopic Investigation, Formal analysis, Funding acquisition, Project administration, Resources, Supervision, Writing – review & editing.

Declaration of Competing Interest

The authors declare that they have no known competing financial

interests or personal relationships that could have appeared to influence the work reported in this paper.

Data availability

Data will be made available on request.

Acknowledgments

The authors are grateful for the financial support from Fundação de Amparo à Pesquisa do Estado de São Paulo (FAPESP: No 2021/08111–2 60 H.F.B., M.C.F.C.F.; 2020/16795–6 L.B.), Conselho Nacional de Desenvolvimento Científico e Tecnológico (CNPq: No. 62 308872/2022–3 H.F.B.; 314032/2021/5 M.C.F.C.F.), the Coordenação de Aperfeiçoamento de Pessoal de Nível Superior (CAPES).

Appendix A. Supporting information

Supplementary data associated with this article can be found in the online version at doi:10.1016/j.jallcom.2024.175319.

References

[1] L.B. Guimarães, A.M.P. Botas, M.C.F.C. Felinto, R.A.S. Ferreira, L.D. Carlos, O. L. Malta, et al., Highly sensitive and precise optical temperature sensors based on new luminescent Tb^{3+}/Eu^{3+}tetrakis complexes with imidazolic counterions, Mater. Adv. 1 (2020) 1988–1995, https://doi.org/10.1039/d0ma00201a.
[2] O.A. Savchuk, J.J. Carvajal, C.D.S. Brites, L.D. Carlos, M. Aguilo, F. Diaz, Upconversion thermometry: a new tool to measure the thermal resistance of nanoparticles, Nanoscale 10 (2018) 6602–6610, https://doi.org/10.1039/c7nr08758f.
[3] S.V. Eliseeva, J.-C.G. Bünzli, Lanthanide luminescence for functional materials and bio-sciences, Chem. Soc. Rev. 39 (2010) 189–227, https://doi.org/10.1039/B905604C.
[4] B.K. Gupta, D. Haranath, S. Saini, V.N. Singh, V. Shanker, Synthesis and characterization of ultra-fine Y_2O_3:Eu^{3+} nanophosphors for luminescent security ink applications, Nanotechnology 21 (2010), https://doi.org/10.1088/0957-4484/21/5/055607.
[5] J.C.G. Bünzli, Lanthanide light for biology and medical diagnosis, J. Lumin 170 (2016) 866–878, https://doi.org/10.1016/j.jlumin.2015.07.033.
[6] R. Ilmi, K. Iftikhar, Photophysical properties of Lanthanide(III) 1,1,1-trifluoro-2,4-pentanedione complexes with 2,2′-Bipyridyl: an experimental and theoretical investigation, J. Photochem. Photobio. A Chem. 333 (2017) 142–155, https://doi.org/10.1016/j.jphotochem.2016.10.014.
[7] L.H.C. Francisco, M.C.F.C. Felinto, H.F. Brito, E.E.S. Teotonio, O.L. Malta, Development of highly luminescent PMMA films doped with Eu^{3+}β-diketonate coordinated on ancillary ligand, J. Mater. Sci. Mater. Electron 30 (2019) 16922–16931, https://doi.org/10.1007/s10854-019-01639-9.
[8] M. Gil-Kowalczyk, R. Łyszczek, A. Jusza, R. Piramidowicz, Thermal, spectroscopy and luminescent characterization of hybrid PMMA/lanthanide complex materials, Mater. (Basel) 14 (2021) 3156, https://doi.org/10.3390/ma14123156.
[9] M.G. Debije, P.P.C. Verbunt, Thirty years of luminescent solar concentrator research: Solar energy for the built environment, Adv. Energy Mater. 2 (2012) 12–35, https://doi.org/10.1002/aenm.201100554.
[10] R.A.S. Ferreira, S.F.H. Correia, A. Monguzzi, X. Liu, F. Meinardi, Spectral converters for photovoltaics – What's ahead, Mater. Today 33 (2020) 105–121, https://doi.org/10.1016/j.mattod.2019.10.002.
[11] I.P. Assunção, I.F. Costa, P.R.S. Santos, E.E.S. Teotonio, M.C.F.C. Felinto, U. Kynast, et al., Luminescent analysis of Eu^{3+} and Tb^{3+} flufenamate Complexes Doped in PMMA polymer: unexpected terbium green emission under sunlight exposure, ACS Appl. Opt. Mater. 1 (2023) 354–366, https://doi.org/10.1021/acsaom.2c00070.
[12] R. Reisfeld, New developments in luminescence for solar energy utilization, Opt. Mater. (Amst.) 32 (2010) 850–856, https://doi.org/10.1016/j.optmat.2010.04.034.
[13] J.-C.G. Bünzli, C. Piguet, Taking advantage of luminescent lanthanide ions, Chem. Soc. Rev. 34 (2005) 1048, https://doi.org/10.1039/b406082m.
[14] K. Binnemans, Interpretation of europium(III) spectra, Coord. Chem. Rev. 295 (2015) 1–45, https://doi.org/10.1016/j.ccr.2015.02.015.
[15] H.F. Brito, O.L. Malta, M.C.F.C. Felinto, E.E.S. Teotonio Luminescence Phenomena Involving Metal Enolates. 2010. https://doi.org/10.1002/9780470682531.pat0419.
[16] K. Binnemans, Rare-earth beta-diketonates, Handb. Phys. Chem. Rare Earths 35 (2005) 107–272, https://doi.org/10.1016/S0168-1273(05)35003-3.
[17] W. Rochowiak, E. Kasprzycka, I.P. Assunção, U. Kynast, M. Lezhnina, Long-lifetime green-emitting Tb^{3+} complexes for bacterial staining, Aust. J. Chem. (2022) 1–6, https://doi.org/10.1071/CH21315.
[18] Y. Yang, K. Wang, D. Yan, Smart luminescent coordination polymers toward multimode logic gates: time-resolved, tribochromic and excitation-dependent fluorescence/phosphorescence emission, ACS Appl. Mater. Interfaces 9 (2017) 17399–17407, https://doi.org/10.1021/acsami.7b00594.
[19] C. Xing, B. Zhou, D. Yan, W. Fang, Integrating full-color 2D optical waveguide and heterojunction engineering in halide microsheets for multichannel photonic logical gates, Adv. Sci. 11 (2024) 2310262, https://doi.org/10.1002/advs.202310262.
[20] C. Xing, B. Zhou, D. Yan, W. Fang, Dynamic photoresponsive ultralong phosphorescence from one-dimensional halide microrods toward multilevel information storage, CCS Chem. 5 (2023) 2866–2876, https://doi.org/10.31635/ccschem.023.202202605.
[21] Y. Yang, K. Wang, D. Yan, A. Manuscript, Lanthanide doped coordination polymers with tunable afterglow based on phosphorescence energy transfer, Chem. Commun. 53 (2017) 7752–7755, https://doi.org/10.1039/C7CC04356B.
[22] Y. Lin, S. Liu, D. Yan, Flexible crystal heterojunctions of low-dimensional organic metal halides enabling color-tunable space-resolved optical waveguides, Article 0259, Research 6 (2023), https://doi.org/10.34133/research.0259.
[23] X. Yang, X. Lin, Y. Zhao, Y.S. Zhao, D. Yan, Lanthanide-organic framework microrods: color tunable optical waveguide and chiral polarized emission, Angew. Chem. Int Ed. 56 (2017) 7853–7857, https://doi.org/10.1002/anie.201703917.
[24] S.I. Weissman, Intramolecular energy transfer. The fluorescence of complexes of europium, J. Chem. Phys. 10 (1942) 214–217, https://doi.org/10.1063/1.1723709.
[25] I.F. Costa, L. Blois, T.B. Paolini, I.P. Assunção, M.C.F.C. Felinto, R.T.M. Jr, et al., Luminescence properties of lanthanide tetrakis complexes as molecular light emitters, Coord. Chem. Rev. 502 (2024) 215590, https://doi.org/10.1016/j.ccr.2023.215590.
[26] G. de Sá, O.L. Malta, C. de Mello Donegá, A.M. Simas, R.L. Longo, P.A. Santa-Cruz, et al., Spectroscopic properties and design of highly luminescent lanthanide coordination complexes, Coord. Chem. Rev. 196 (2000) 165–195, https://doi.org/10.1016/S0010-8545(99)00054-5.
[27] O.L. Malta, Ligand—rare-earth ion energy transfer in coordination compounds. A theoretical approach, J. Lumin 71 (1997) 229–236, https://doi.org/10.1016/S0022-2313(96)00126-3.
[28] G.E. Buono-core, H. Li, B. Marciniak, Quenching of excited states by lanthanide ions and chelates in solution, Coord. Chem. Rev. 99 (1990) 55–87, https://doi.org/10.1016/0010-8545(90)80060-7.
[29] W.M. Faustino, G.F. de Sá Intramolecular energy transfer through charge transfer state in lanthanide compounds: A theoretical approach Intramolecular energy transfer through charge transfer state in lanthanide compounds: A theoretical approach 2005;54109. https://doi.org/10.1063/1.1830452.
[30] G.A. Crosby, R.E. Whan, J.J. Freeman, Spectroscopic studies of rare earth chelates, J. Phys. Chem. 66 (1962) 2493–2499, https://doi.org/10.1021/j100818a041.
[31] R.E. Whan, G.A. Crosby, 1962_Luminescence studies of rare earth complexes: benzoylacetonate and dibenzoylmethide chelates, J. Mol. Spectrosc. 8 (1962) 315–327, https://doi.org/10.1016/0022-2852(62)90031-0.
[32] R.D. Adati, J.H.S.K. Monteiro, The influence of different ammonium cations on the optical properties of tetrakis Gd, J. Braz. Chem. Soc. 30 (2019) 1707–1716, https://doi.org/10.21577/0103-5053.20190073.
[33] J. Kai, M.C.F.C. Felinto, L. a O. Nunes, O.L. Malta, H.F. Brito, Intermolecular energy transfer and photostability of luminescence-tuneable multicolour PMMA films doped with lanthanide–β-diketonate complexes, J. Mater. Chem. 21 (2011) 3796, https://doi.org/10.1039/c0jm03474f.
[34] R. Brighenti, Y. Li, F.J. Vernerey, Smart polymers for advanced applications: a mechanical perspective review, Front Mater. 7 (2020) 1–18, https://doi.org/10.3389/fmats.2020.00196.
[35] W.S.P. Carvalho, M. Wei, N. Ikpo, Y. Gao, M.J. Serpe, Polymer-based technologies for sensing applications, Anal. Chem. 90 (2018) 459–479, https://doi.org/10.1021/acs.analchem.7b04751.
[36] S.A. Gârea, A.I. Voicu, H. Iovu, Clay–polymer nanocomposites for controlled drug release. Clay-Polymer Nanocomposites, Elsevier, 2017, pp. 475–509, https://doi.org/10.1016/B978-0-323-46153-5.00014-8.
[37] P.K. Deb, S.F. Kokaz, S.N. Abed, A. Paradkar, R.K. Tekade, Pharmaceutical and biomedical applications of polymers. basic fundam. Drug Deliv., Elsevier, 2019, pp. 203–267, https://doi.org/10.1016/B978-0-12-817909-3.00006-6.
[38] A. Sikder, A.K. Pearce, S.J. Parkinson, R. Napier, R.K. O'Reilly, Recent trends in advanced polymer materials in agriculture related applications, ACS Appl. Polym. Mater. 3 (2021) 1203–1217, https://doi.org/10.1021/acsapm.0c00982.
[39] M. Gubišová, M. Hudcovicová, P. Matušinský, K. Ondreičková, L. Klčová, J. Gubiš, Superabsorbent polymer seed coating reduces leaching of fungicide but does not alter their effectiveness in suppressing pathogen infestation, Polym. (Basel) 14 (2021) 76, https://doi.org/10.3390/polym14010076.
[40] Z. Huang, M. Shanmugam, Z. Liu, A. Brookfield, E.L. Bennett, R. Guan, et al., Chemical recycling of polystyrene to valuable chemicals via selective acid-catalyzed aerobic oxidation under visible light, J. Am. Chem. Soc. 144 (2022) 6532–6542, https://doi.org/10.1021/jacs.2c01410.
[41] X. Yang, Y. Wang, Y. Zhou, J. Chen, Q. Wan, The application of polycaprolactone in three-dimensional printing scaffolds for bone tissue engineering, Polym. (Basel) 13 (2021), https://doi.org/10.3390/polym13162754.
[42] T. Soganci, Y. Baygu, Y. Gök, M. Ak, Disulfide-linked symmetric N-alkyl carbazole derivative as a new electroactive monomer for electrochromic applications, Synth. Met 244 (2018) 120–127, https://doi.org/10.1016/j.synthmet.2018.07.009.
[43] D. Sun, Z. Ren, M.R. Bryce, S. Yan, Arylsilanes and siloxanes as optoelectronic materials for organic light-emitting diodes (OLEDs), J. Mater. Chem. C. 3 (2015) 9496–9508, https://doi.org/10.1039/c5tc01638j.
[44] R. Pernites, R. Ponnapati, M.J. Felipe, R. Advincula, Electropolymerization molecularly imprinted polymer (E-MIP) SPR sensing of drug molecules: pre-polymerization complexed terthiophene and carbazole electroactive monomers,

Biosens. Bioelectron. 26 (2011) 2766–2771, https://doi.org/10.1016/j.bios.2010.10.027.
[45] J.C.G. Bünzli, On the design of highly luminescent lanthanide complexes, Coord. Chem. Rev. 293–294 (2015) 19–47, https://doi.org/10.1016/j.ccr.2014.10.013.
[46] P. Forget, C. Bentin, J.-P. Machiels, M. Berliere, P.G. Coulie, M. De Kock, Intraoperative use of ketorolac or diclofenac is associated with improved disease-free survival and overall survival in conservative breast cancer surgery, Br. J. Anaesth. 113 (2014) i82–i87, https://doi.org/10.1093/bja/aet464.
[47] S.R. Chirasani, P. Leukel, E. Gottfried, J. Hochrein, K. Stadler, B. Neumann, et al., Diclofenac inhibits lactate formation and efficiently counteracts local immune suppression in a murine glioma model, Int J. Cancer 132 (2012) 843–853, https://doi.org/10.1002/ijc.27712.
[48] Z. Varga, S. rafay ali Sabzwari, V. Vargova, Cardiovascular risk of nonsteroidal anti-inflammatory drugs: an under-recognized public health issue, Cureus 9 (2017), https://doi.org/10.7759/cureus.1144.
[49] P.L. Temporelli, G.B. Zito, R.F. Pedretti, F.I. Belisarii, G. Putortì, P. Faggiano, Nonsteroid anti-inflammatory drugs (NSAID) and risk of cardiovascular events. Literature review and clinical implications, Monaldi Arch. Chest Dis. 82 (2015) 165–170, https://doi.org/10.4081/monaldi.2014.58.
[50] C.N. Banti, S.K. Hadjikakou, Non-steroidal anti-inflammatory drugs (NSAIDs) in metal complexes and their effect at the cellular level, Eur. J. Inorg. Chem. 2016 (2016) 3048–3071, https://doi.org/10.1002/ejic.201501480.
[51] I.P. Assunção, M. Bredol, E. Kasprzycka, U.H. Kynast, M. Lezhnina, Near-UV-excitable, green-emitting Tb^{3+}-based complexes, Inorg. Chim. Acta 515 (2021) 120071, https://doi.org/10.1016/j.ica.2020.120071.
[52] E. Kasprzycka, I.P. Assunção, M. Bredol, M. Lezhnina, U.H. Kynast, Preparation, characterization and optical properties of rare earth complexes with derivatives of n-phenylanthranilic acid preparation, characterization and optical properties of rare earth complexes with derivatives of n-phenylanthranilic acid, J. Lumin 232 (2021) 117818, https://doi.org/10.1016/j.jlumin.2020.117818.
[53] V.F. Zolin, V.I. Tsaryuk, V.A. Kudryashova, K.P. Zhuravlev, P. Gawryszewska, J. Legendziewicz, et al., Spectroscopy of Eu^{3+} and Tb^{3+} pyridine- and pyrazine-2-carboxylates, J. Alloy. Compd. 451 (2008) 149–152, https://doi.org/10.1016/j.jallcom.2007.04.125.
[54] J.H. Hong, Y. Oh, Y. Kim, S.K. Kang, J. Choi, W.S. Kim, et al., Polymorph selective growth of sodium tetrakis(2-pyridinecarboxylato) lanthanides and their structure sensitive properties, Cryst. Growth Des. 8 (2008) 1364–1371, https://doi.org/10.1021/cg7012705.
[55] S. Li, Y. Wang, Q. Lin, W. Liu, J. Ding, Y. Wang, Synthesis, crystal structures of novel complexes of rare earth with norfloxacin, interaction with DNA and BSA, J. Rare Earths 30 (2012) 460–466, https://doi.org/10.1016/S1002-0721(12)60073-8.
[56] R. Janicki, A. Mondry, P. Starynowicz, Carboxylates of rare earth elements, Coord. Chem. Rev. 340 (2017) 98–133, https://doi.org/10.1016/j.ccr.2016.12.001.
[57] I.P. Assunção, A.N. Carneiro Neto, R.T. Moura, C.C.S. Pedroso, I.G.N. Silva, M.C.F.C. Felinto, et al., Odd-even effect on luminescence properties of europium aliphatic dicarboxylate complexes, ChemPhysChem 20 (2019) 1931–1940, https://doi.org/10.1002/cphc.201900603.
[58] Y. Hasegawa, T. Nakanishi, Luminescent lanthanide coordination polymers for photonic applications, RSC Adv. 5 (2015) 338–353, https://doi.org/10.1039/c4ra09255d.
[59] T. Rhauderwiek, C. dos Santos Cunha, H. Terraschke, N. Stock, Bismuth coordination polymers with 2,4,6-pyridine tricarboxylic acid: high-throughput investigations, crystal structures and luminescence properties, Eur. J. Inorg. Chem. 2018 (2018) 3232–3240, https://doi.org/10.1002/ejic.201800154.
[60] De Oliveira, C.A.F. Silva, F.F. Da, I. Malvestiti, V.R.D.S. Malta, J.D.L. Dutra, N.B. Da Costa, et al., Synthesis, characterization, luminescent properties and theoretical study of two new coordination polymers containing lanthanide [Ce(III) or Yb(III)] and succinate ions, J. Mol. Struct. 1041 (2013) 61–67, https://doi.org/10.1016/j.molstruc.2013.03.001.
[61] A. Topacli, S. Ide, Molecular structures of metal complexes with mefenamic acid, J. Pharm. Biomed. Anal. 21 (1999) 975–982, https://doi.org/10.1016/S0731-7085(99)00198-3.
[62] L. Zapała, M. Kosińska, E. Woźnicka, Ł. Byczyński, W. Zapała, Synthesis, spectral and thermal study of La(III), Nd(III), Sm(III), Eu(III), Gd(III) and Tb(III) complexes with mefenamic acid, J. Therm. Anal. Calor. 124 (2016) 363–374, https://doi.org/10.1007/s10973-015-5120-0.
[63] H. Bojarowicz, Z. Kokot, A. Surdykowski, Complexes of Fe(III) ions with mefenamic acid, J. Pharm. Biomed. Anal. 15 (1996) 339–342, https://doi.org/10.1016/S0731-7085(96)01873-0.
[64] S. Jabeen, T.J. Dines, S.A. Leharne, B.Z. Chowdhry, Spectrochimica acta part a: molecular and biomolecular spectroscopy raman and ir spectroscopic studies of fenamates – conformational differences in polymorphs of flufenamic acid, mefenamic acid and tolfenamic acid, Spectrochim. Acta Part A Mol. Biomol. Spectrosc. 96 (2012) 972–985, https://doi.org/10.1016/j.saa.2012.07.129.
[65] R.K. Gilpin, W. Zhou, Infrared studies of the polymorphic states of the fenamates, J. Pharm. Biomed. Anal. 37 (2005) 509–515, https://doi.org/10.1016/j.jpba.2004.11.009.
[66] G. Deacon, Relationships between the carbon-oxygen stretching frequencies of carboxylato complexes and the type of carboxylate coordination, Coord. Chem. Rev. 33 (1980) 227–250, https://doi.org/10.1016/S0010-8545(00)80455-5.
[67] K.P. Zhuravlev, Ł. Michnik, P. Gawryszewska, V.I. Tsaryuk, V.A. Kudryashova, Europium and terbium pyrrole-2-carboxylates: structures, luminescence, and energy transfer, Inorg. Chim. Acta 492 (2019) 1–7, https://doi.org/10.1016/j.ica.2019.04.014.
[68] K.P. Zhuravlev, V.I. Tsaryuk, V.A. Kudryashova, Photoluminescence of europium and terbium trifluoroacetylacetonates. Participation of LMCT state in processes of the energy transfer to Eu^{3+} ion, J. Fluor Chem. 212 (2018) 137–143, https://doi.org/10.1016/j.jfluchem.2018.06.002.
[69] M.G. Lahoud, R.C.G. Frem, D.A. Gálico, G. Bannach, M.M. Nolasco, R.A.S. Ferreira, et al., Intriguing light-emission features of ketoprofen-based Eu(III) adduct due to a strong electron–phonon coupling, J. Lumin 170 (2016) 357–363, https://doi.org/10.1016/j.jlumin.2015.08.050.
[70] Carnall W.T., Crosswhite H., Crosswhite H.M. Energy level structure and transition probabilities in the spectra of the trivalent lanthanides in LaF_3. Argonne, IL (United States): 1978. https://doi.org/10.2172/6417825.
[71] G.B.V. Lima, J.C. Bueno, A.F. da Silva, A.N. Carneiro Neto, R.T. Moura, E.E. S. Teotonio, et al., Novel trivalent europium β-diketonate complexes with N-(pyridine-2-yl)amides and N-(pyrimidine-2-yl)amides as ancillary ligands: photophysical properties and theoretical structural modeling, J. Lumin 219 (2020), https://doi.org/10.1016/j.jlumin.2019.116884.
[72] A.N. Carneiro Neto, E.E.S. Teotonio, G.F. de Sá, H.F. Brito, J. Legendziewicz, L.D. Carlos, et al. Modeling intramolecular energy transfer in lanthanide chelates: A critical review and recent advances. vol. 56, 2019, p. 55–162. https://doi.org/10.1016/bs.hpcre.2019.08.001.
[73] R.T. Moura, A.N. Carneiro Neto, R.L. Longo, O.L. Malta, On the calculation and interpretation of covalency in the intensity parameters of 4f–4f transitions in Eu^{3+} complexes based on the chemical bond overlap polarizability, J. Lumin (2015) 1–11, https://doi.org/10.1016/j.jlumin.2015.08.016.
[74] A. Shyichuk, R.T. Moura, A.N. Carneiro Neto, M. Runowski, M.S. Zarad, A. Szczeszak, et al., Effects of dopant addition on lattice and luminescence intensity parameters of Eu(III)-doped lanthanum orthovanadate, J. Phys. Chem. C. 120 (2016) 28497–28508, https://doi.org/10.1021/acs.jpcc.6b10778.
[75] H.F. Brito, O.M.L. Malta, M.C.F.C. Felinto, E.E.S. Teotônio, Luminescence Phenomena Involving Metal Enolates. PATAI'S. Chem. Funct. Groups, John Wiley & Sons, Ltd, Chichester, UK, 2010, p. 1210, https://doi.org/10.1002/9780470682531.pat0419.
[76] P.P. Barthelemy, G.R. Choppin, Luminescence study of complexation of europium and dicarboxylic acids, Inorg. Chem. 28 (1989) 3354–3357, https://doi.org/10.1021/ic00316a023.